

Nonmonotonic behavior in the dense assemblies of active colloids

Natsuda Klongvessa,¹ Félix Ginot,^{1,*} Christophe Ybert,¹ Mathieu Leocmach,¹ and Cécile Cottin-Bizonne^{1,†}

¹*Université de Lyon, Université Claude Bernard Lyon 1, CNRS,
Institut Lumière Matière, F-69622, VILLEURBANNE, France*

We study experimentally a sediment of self-propelled Brownian particles with densities ranging from dilute to ergodic supercooled to nonergodic glass. We observe a dramatic slowdown of relaxation of nonergodic states when particles become weakly self-propelled. By contrast, ergodic supercooled states always relax faster with self-propulsion. Our system is a monolayer of micron-size gold-platinum Janus particles, which become active upon adding a solution of hydrogen peroxide due to self-phoretic propulsion mechanisms. We characterise the activity level in our system with an effective temperature defined from the density profile. Standard glassy physics describes well the ergodic regime provided the replacement of the ambient temperature by this effective temperature: higher temperature implies faster relaxation. However beyond the glass transition, the relaxation of the nonergodic system abruptly slows down at low but nonzero activity. As we increase further activity, the relaxation speeds up until it exceeds the passive situation. This nonmonotonic behavior cannot be described by a simple increase in temperature. To explain this phenomenon, we correlated particle displacement orientation and calculated the average length of correlated domains. It shows first a decrease and then an increase with the effective temperature. In particular, the minimum correlated domain length corresponds to the effective temperature where we detected the slowest relaxation. This suggests that relaxation in sufficiently active glass follows collective motion mechanisms, while cooperative motion dominates at zero and low activities. We propose that directed motion makes cage exploration less efficient and thus slows down cooperative relaxation with respect to a passive glass.

INTRODUCTION

In the last decade, the mesmerizing dynamic patterns of bird flocks has become a rallying sign for a large community of physicists [1]. The growing field of active matter deals with the statistical physics of self-propelled objects and has deep implications from crowd dynamics, to energy harvesting, to cancer metastasis. Active systems are driven out of equilibrium by energy injected at the level of the individual particle [2–4]. Despite their intrinsically nonequilibrium nature, effective thermodynamic variables, e.g. an effective temperature, can be defined to map different steady-state behaviors of active systems onto equilibrium concepts: sedimentation-diffusion [5], phase separation [6–8], or crystallization [8, 9]. However many collective behaviors emerging from self-propelled systems have no equilibrium equivalent: giant density fluctuations [10], clustering [11, 12], travelling polar phase [13] or turbulence [14].

In this context, the possibility of such a mapping for the glass transition of active systems is still debated. Numerical studies found that despite a quantitative shift of the glass transition line, the qualitative phenomenology of glassiness remained unchanged [15]. In a letter accompanying this article, we show experimentally a non-monotonic response of the dynamics of a glass to low levels of self-propulsion [16]. In the present article, we discuss more in depth the conditions where the behavior of glassy systems can be mapped to a passive counterpart, and the microscopic mechanisms that explain the failure of the mapping.

When a liquid is cooled down, or when a suspension

becomes denser, their dynamics slow down by orders of magnitude, until the system cannot be equilibrated in a reasonable time. The resulting system is nonergodic, which means that it can explore only a small part of the phase space. Our understanding of glass as a fundamental state of matter, and of the dynamical arrest that lead to it has tremendously progressed in the last decades [17, 18].

The first numerical study of glassy systems of self-propelled particles used the Active Brownian Particle (ABP) model, where the particles are submitted both to propulsion forces and temperature-induced Brownian agitation [19]. Colloidal particles that self-propel by self-phoretic mechanisms are well described by ABP model [5, 11, 20]. An effective temperature can be defined for ABP that takes into account both the temperature of the bath and the characteristics of the propulsion force [5, 21]. For simplicity, later models discarded the thermal bath and kept only various implementations of a persistent propulsion force [15, 22–25]. Each of these models can be unambiguously assigned an effective temperature. Depending on the numerical model, a rise of effective temperature can either lead to activity-induced fluidization [19, 22] or arrest [23, 24]. It was found that the glass transition line shifted in nontrivial ways with the persistence time of the propulsion direction. The influence of activity could thus not be captured by a single parameter such as effective temperature. For example in Ref. [15] glass transition shifts to higher densities with increasing persistence time if the effective temperature is low, but to lower densities if the effective temperature is high. Indeed, Nandi *et al.* [25] have recently shown

analytically that the monotonicity of the glass transition shift depends on the microscopic details of the activity.

The focus of the above-cited numerical and analytical studies was on the position of the glass transition line, inferred by an approach from the ergodic supercooled state, and not on the nonergodic state beyond this line. This is precisely beyond this ergodic to nonergodic line that we find experimentally a nontrivial phenomenology that cannot be mapped to a passive counterpart. In the accompanying letter [16], we study the influence of self-propulsion on a sediment of Brownian particles, in order to access states on both sides of the nonergodic glass transition. We show that the relaxation of the supercooled liquid speeds up with activity, whereas the nonergodic glass displays a slowdown upon introduction of low levels of activity, but a speedup at higher activity levels. In the present article, we reexamine the experimental conditions where we observe this nonmonotonic response. We then perform careful measurements of effective temperature and density in order to map the ergodic supercooled regime at various activity levels onto the passive case. The failure of this mapping beyond the glass transition motivates an investigation of the microscopic relaxation mechanisms. Experimentally, we distinguish cooperative and collective motions and show analytically why even extremely low levels of self-propulsion hinder cooperative relaxation. We finally discuss our results in the light of passive glass theoretical framework.

EXPERIMENTAL SET-UP

We make Janus particles starting from gold particles (Bio-Rad #1652264) of diameter $1.6\ \mu\text{m}$ that we half coat with $20\ \text{nm}$ platinum following the method in Ref. [26]. After purification and sorting, the Janus particles dispersed in deionized water are put into a well (Falcon #353219). Due to their high density $\rho \simeq 11\ \text{g cm}^{-3}$, particles settle down to the bottom to form a monolayer. We observe their 2D motion from below on a Leica DMI 4000B microscope equipped by an external dark-field lightning ring and a Basler camera (acA2040-90um). Video data are taken at 5 and $20\ \text{Hz}$ and analyzed using Trackpy package [27].

Since the colloidal particles are charged and the ionic force of the solvent is low, electrostatic repulsion prevents direct contact between particles. We estimate an effective diameter of the particles to $\sigma_0 = 2.2\ \mu\text{m}$ from the position of the first peak of the radial pair correlation function in a dense passive regime. This allows us to define the area fraction as $\phi = 4\rho/(\pi\sigma_0^2)$, where ρ is the number density. However $\sigma_0/2$ is larger than the hydrodynamic radius of the particles R_H . From the translational diffusion coefficient in dilute conditions, we estimate $R_H \approx 0.94\ \mu\text{m}$, which corresponds to an inertial time $\tau_\nu = (2\rho R_H^2)/(9\eta) \approx 2\ \mu\text{s}$, a Brownian translational

time $\tau_T = (3\pi\eta R_H^3)/(2k_B T_0) \approx 0.9\ \text{s}$ and a Brownian rotational time $\tau_R = (8\pi\eta R_H^3)/(k_B T_0) \approx 5\ \text{s}$, where T_0 is the bath temperature. Unless stated otherwise, in the following we normalize distances by σ_0 , and times by τ_R .

Self-propulsion is made possible in dilute hydrogen peroxide (H_2O_2 , Merck Millipore, #1072090250) solutions by a combination of electrophoresis and diffusiophoresis effects [28, 29]. The two halves of the catalytic splitting of H_2O_2 occur respectively on each side of the particle, causing self-phoretic effects that drive the particle forward. In dilute regime, the mean square displacement (MSD, see Fig. 1a) displays ballistic motion at short times and diffusive motion at long times due to rotational diffusion. The rotational diffusion time is practically independent on H_2O_2 concentration, and approximately equal to τ_R . By contrast, the propulsion velocity increases monotonically with H_2O_2 concentration, up to $10\ \mu\text{m s}^{-1}$ at $0.1\ \text{v/v}\ \%$ concentration. We extract the effective diffusion coefficient, D_{eff} , of this persistent random motion by fitting the long-time scale MSD and show in the inset that it increases monotonically with H_2O_2 concentration.

Due to the large volume of solvent above the monolayer, we find that the effects of activity are stable in time over the course of several hours. In particular, purely diffusive motion could be recovered only several days after the last H_2O_2 introduction. That is why we always wash several times our particles with milliQ water before starting a series of experiments and always increase step by step H_2O_2 concentration from that clean state. At each step, acquisition is started 30 minutes after H_2O_2 introduction to allow a steady state to be reached.

In-plane sedimentation is obtained by tilting the whole set-up with a small angle $\theta \approx 0.1^\circ$, see the sketch of the set-up in Fig. 1b. The monolayer of particles is thus under an in-plane gravity $g \sin \theta \approx 2 \times 10^{-2}\ \text{m/s}^2$. The sample is mounted on a motorized XY translation stage (SCAN IM 130x85) that we program for systematic observations at different heights of the sediment with positioning repeatability below $1\ \mu\text{m}$ while minimizing in-plane acceleration.

In the following we will first focus on the densest part of the sediment as we progressively increase activity to characterize its dynamics, effective temperature and density. Then, we will take a broader look at the whole sediment to characterize the system at all densities. In particular, we will characterize dynamics on both sides of the glass transition. Finally, we will focus on the relaxation mechanisms of the nonergodic region and build an analytical model to explain our observations.

DENSE ACTIVE BEHAVIOR

The black curve in Fig. 1b shows the MSD of the densest part of the sediment before any H_2O_2 addition (curve #1). The plateau is typical of glassy behavior and indi-

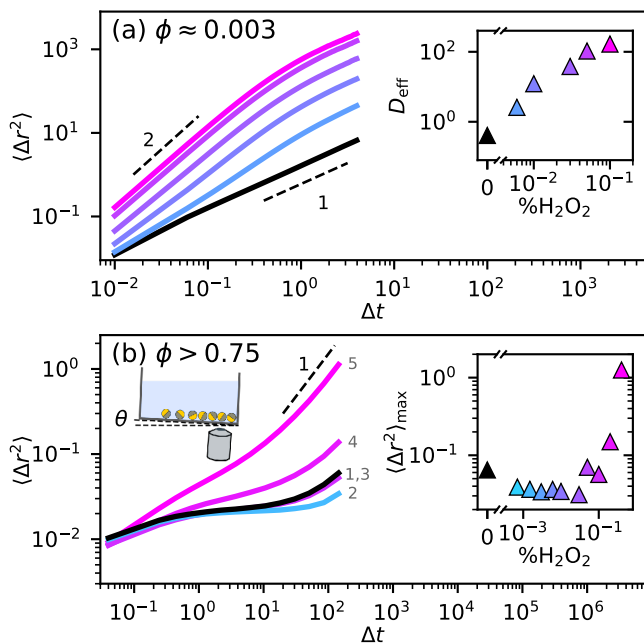


FIG. 1. Characterization of active colloid motion in dilute (a) and dense (b) regimes at various H_2O_2 concentrations increasing from black (without H_2O_2), to cyan to magenta, see respective insets. (a) Mean square displacement in the dilute regime. Dashed lines indicate slopes 1 (diffusive motion) and 2 (ballistic motion). Inset: Corresponding effective diffusion coefficient versus H_2O_2 concentration, extracted from the long-time MSD. (b) Mean square displacement in the dense regime. The numbers denote the order of increment of H_2O_2 concentration. To increase readability, intermediate concentrations between #2 and #3 are not shown, since their curves are almost identical to #2. The experimental set-up to obtain the dense regime by tilting the microscope together with the sample is sketched. Note that the set-up is not tilted in (a). Inset: Values of MSD at the longest lag time.

cates that each particle is trapped by its neighbors. At long times, the system exits the plateau hinting that the particles manage to diffuse away from their original positions [30].

As we introduce a small amount of H_2O_2 , the plateau gets longer, as shown on curve #2 in Fig. 1b. This surprisingly indicates that the system is less mobile when each particle is weakly self-propelled. However, when H_2O_2 is further increased, we recover a mobility equivalent to the passive case (curve #3). At even higher concentrations, the system has more and more mobility. The plateau becomes shorter (curve #4) and finally disappear (curve #5) where we can observe an effective diffusion motion at long time scale.

In the inset of Fig. 1b, this nonmonotonic behavior is quantified at more values of H_2O_2 concentration by the value of MSD at the maximum lag time. Indeed, at concentrations of H_2O_2 lower than $\approx 0.04\%$ the system is more arrested than in the passive case, but diffusion

become more effective over $\approx 0.10\%$. We call this behavior ‘back and forth’ behavior. The ‘back’ behavior is when the mobility of the system decreases lower than the passive case, whereas in the ‘forth’ regime the system is fluidized by activity.

In the following we will try to understand in which conditions the mobility of the system does depend non-monotonically on the activity level.

EFFECTIVE TEMPERATURE AND COMPACTION

First, we have to make sure that ‘activity’ is monotonic with H_2O_2 concentration. Theoretically, the activity of self-propelled particles of mass m and mobility μ can be characterized by two scalars among propulsion force F_P , persistence time τ_P or propulsion temperature T_P [15, 24, 25] such that

$$k_B T_P = \frac{1}{2} m \left(\frac{F_P}{\mu} \right)^2, \quad (1)$$

where k_B is the Boltzmann constant. Experimentally, our particles are submitted to both Brownian and active motions. Here we make the hypothesis that the persistence time is fixed by Brownian rotational diffusion and thus practically constant $\tau_P = \tau_R$, as confirmed in dilute conditions. We cannot measure directly F_P or T_P in a dense sediment. However we have access to an effective temperature (T_{eff}) measured from the dilute limit of the sedimentation profile, as described in [20]. From the sedimentation experiment on passive colloids [31], the competition between diffusive motion and gravity g results in a density profile that has the Boltzmann form at low enough densities: $\phi(x) \sim \exp[mgx/D_0\mu]$, where x is the coordinate in the direction of gravity, $D_0 = k_B T_0/\mu$ is the diffusion coefficient. Following Refs [5, 32], in the case of self-propelled particles D_0 can be replaced by the long time effective diffusion coefficient $D_{\text{eff}}(\phi \rightarrow 0)$, or equivalently T_0 can be replaced by an effective temperature such that $k_B T_{\text{eff}} \equiv \mu D_{\text{eff}}(\phi \rightarrow 0)$. This amounts to viewing a dilute active system as ‘hot colloids’ with an effective temperature.

This effective temperature can be related to the propulsion temperature T_P by expressing the long term diffusion coefficient in dilute regime. Following [5, 21] we use the case of spherical particles undergoing both Brownian and self-propelled motions in 2D but with two degrees of rotational freedom:

$$D_{\text{eff}}(\phi \rightarrow 0) = D_0 + \frac{1}{6} \left(\frac{F_P}{\mu} \right)^2 \tau_R. \quad (2)$$

We can combine (Eq. 1) and (Eq. 2) to get

$$\frac{T_{\text{eff}}}{T_0} = \frac{D_{\text{eff}}}{D_0} = 1 + \frac{1}{3} \frac{\tau_R}{\tau_\nu} \frac{T_P}{T_0}. \quad (3)$$

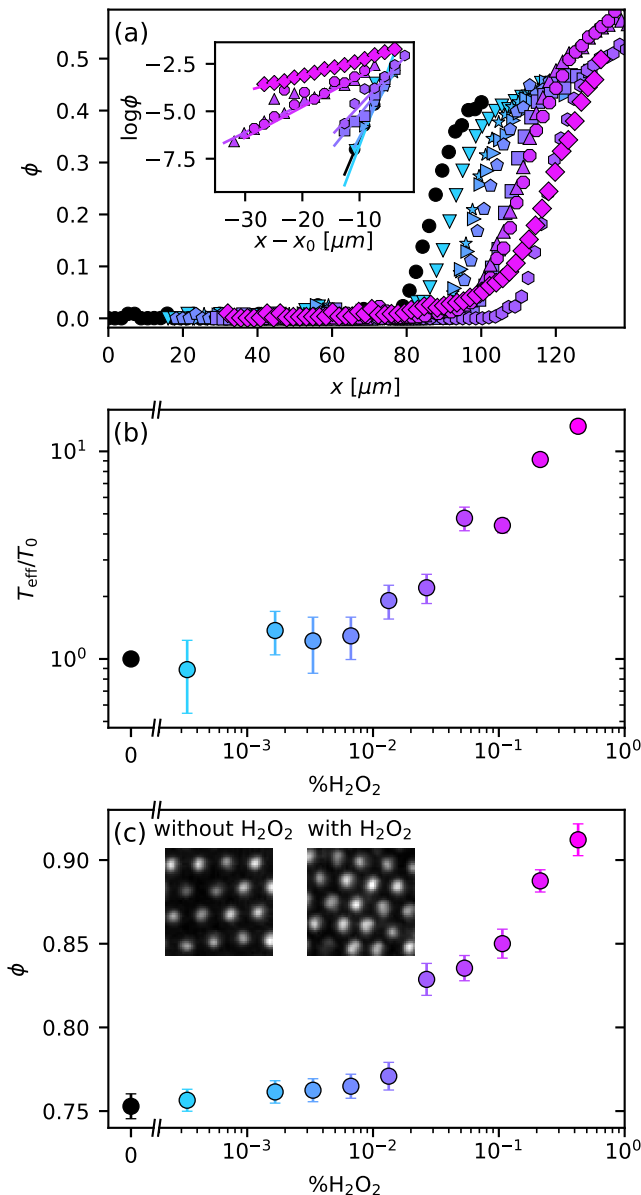


FIG. 2. (a) Density profile, $\phi(x)$, at the top of the sediment for various H_2O_2 concentration color-coded as in Fig. 1b. (inset) Linear fit of $\log \phi$ in order to obtain the ratio between the effective temperature and the Brownian temperature, T_{eff}/T_0 . The abscissa is shifted by x_0 , the position where the profile has the maximum slope. The uncertainty is higher for the passive and low activity cases, where the density profile is sharp and the dilute region is very limited. (b) Calibration of T_{eff}/T_0 versus H_2O_2 concentration. The error bar comes from the uncertainty on the slope measurement. (c) Area density function versus H_2O_2 concentration. (inset) Details of experimental images showing the same compaction.

This equation highlights the importance of persistence time, that amplifies the effect of propulsion temperature. Here, the ratio of the persistence time by the inertial time is so large that a propulsion temperature of the order of $4 \times 10^{-6} T_0$ doubles the effective temperature. In the following we will use T_{eff} to characterize also activity levels in the dense regime.

For each H_2O_2 concentration, to characterize the very same experimental conditions, we acquire data at two fixed locations: one near the bottom (dense regime) and then immediately one at the top of the sediment (dilute regime). From the latter, we obtain the density profiles shown in Fig. 2a. Low density regime indeed displays an exponential dependence (inset) from which we extract T_{eff}/T_0 . The effective temperature dependence on H_2O_2 concentration is monotonic, as shown in Fig. 2b. Using (Eq. 3), we deduce that T_P is also monotonic, with maximum values below $4 \times 10^{-5} T_0$.

In Fig. 2a we notice that the sedimentation profiles shift toward larger x with increasing H_2O_2 concentration. This compaction of the sediment is confirmed by measuring the average density in the bottom part, see Fig. 2c. The particle density rises by about 15% from the passive to the highest activity and we observe that the inter-particle distance also becomes smaller (inset). Compaction could be due to purely chemical effects caused by the increase of H_2O_2 concentration, or could be a general feature of self-propelled particles confined by an external potential. More probably it is a combination between these two factors, as we observe that a sediment of uncoated gold particles does compact with H_2O_2 concentration but by only 4%. This would also be consistent with the double origin of effective attraction observed in the same system [20].

In any case, glassy phenomenology is extremely sensitive to density variations and we have thus to control for this parameter before reaching to any conclusion.

DENSITY CONTROLLED INVESTIGATION

We thus perform another set of experiments where we observe the whole density profile. We divide the sediment into thin slices perpendicular to the gravitational gradient (see Fig. 3a). We set the width of each slice so that every slice contains approximately the same number of particles (1000 ± 100 particles per slice). We can compute all static and dynamic quantities function of the density, parameterized by the altitude x . For instance, we define a microscopic overlap function $w_i(t_0, \Delta t) = \Theta(a - \|\vec{r}_i(t_0 + \Delta t) - \vec{r}_i(t_0)\|)$ that indicates whether particle i has not moved further than $a = 0.3\sigma_0$ between times t_0 and $t_0 + \Delta t$. Here Θ is the Heaviside step function. In each slice, we compute the overlap function [33], $F(\Delta t)$, which tells us the ratio of particles that

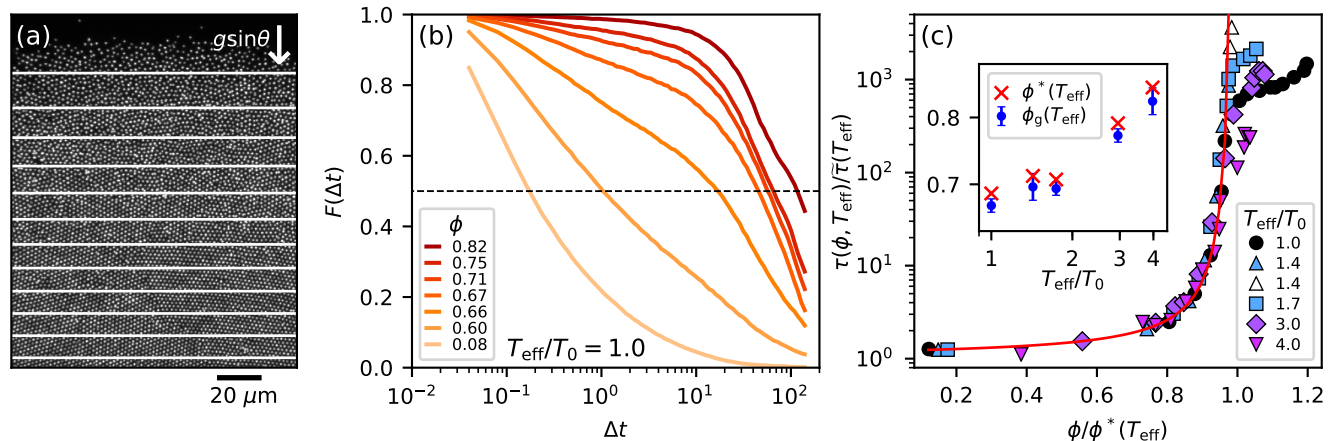


FIG. 3. (a) Experimental image of the sediment showing the slicing to get access to different densities. (b) Overlap function $F(\Delta t)$ in the passive case and at various densities. The dashed line at 0.5 is the threshold where the relaxation time τ is defined. (c) Collapse of density dependence of relaxation time on Eq. 5 (red curve). Beyond glass transition collapse is lost and saturation level follows a nonmonotonic trend with activity. Open triangles are obtained by extrapolation of $F(\Delta t)$. Inset: Ideal and operational glass transition volume fractions, ϕ^* and ϕ_g respectively, function of activity.

have not moved:

$$F(\Delta t) = \left\langle \sum_{i=1}^N w_i(t_0, \Delta t) \right\rangle. \quad (4)$$

Fig. 3b shows $F(\Delta t)$ at various densities of the passive sediment. At high densities, we observe a two-step relaxation typical of glassy dynamics. We note that contrary to systems with a steep repulsive potential, here the height of the plateau depends on density. The plateau completely disappears at the lowest density, and $F(\Delta t)$ relaxes in a single exponential step indicating nonglassy behavior. We define the relaxation time τ when half of the particles have already relaxed, i.e., $F(\tau) = 0.5$ (horizontal dashed line).

When plotting the volume fraction dependence of τ in Fig. 3c, the supercooled and glassy regimes are clearly delimited by the operational glass transition volume fraction ϕ_g , that is the volume fraction at which the system becomes nonergodic. For $\phi < \phi_g$, the relaxation time rises steeply with ϕ , whereas for $\phi > \phi_g$ τ only depends weakly on ϕ . This trend contradicts the usual picture of glass transition where the relaxation time should diverge. However, our phenomenology is consistent with what Philippe *et al.* [34] have observed in a large variety of passive systems made of soft particles.

For each activity, we fit the relaxation time below ϕ_g with the expression

$$\frac{\tau(\phi, T_{\text{eff}})}{\tilde{\tau}(T_{\text{eff}})} = \exp \left[\frac{A}{(\phi^*(T_{\text{eff}})/\phi) - 1} \right], \quad (5)$$

where $A \approx 0.19$ is independent of activity, whereas $\tilde{\tau}(T_{\text{eff}})$ and $\phi^*(T_{\text{eff}})$ are activity-dependent parameters, respectively the relaxation time in the dilute limit and ideal glass transition volume fraction. The collapse of

the supercooled regimes in Fig. 3c indicates that ϕ^* and $\tilde{\tau}$ are enough to describe the physics of glass transition below ϕ_g .

However, this collapse does not hold beyond the glass transition. The inset of Fig. 3c shows our estimate of ϕ_g as where the data departs from the master curve for each activity. Above ϕ_g , in the nonergodic regime, $\tau/\tilde{\tau}$ saturates. This saturation value is different at each activity. It suggests that $\tilde{\tau}(T_{\text{eff}})$ and thus an effective temperature is not enough to describe the effects of self-propulsion on the nonergodic glass. Moreover, this saturation value follows the ‘back and forth’ behavior: an order of magnitude jump between the passive case and the first nonzero activity, and then a decrease with increasing activity. We are thus confident that this nonmonotonic behavior originates directly from the particle self-propulsion and is neither a pure effect of compaction nor reducible to an increase in (effective) temperature. In the following, we focus on two fixed density regimes, just below and just above ϕ_g to understand what makes the special response of the nonergodic glassy system to weak self-propulsion.

In Fig. 4 we show $F(\Delta t)$ and MSD for various activities but at two fixed densities, below and above $\phi_g(T_0) = 0.67$. At $\phi = 0.65 \pm 0.02 < \phi_g(T_0)$ (Fig. 4a), the shape of $F(\Delta t)$ evolves monotonically with T_{eff}/T_0 . The plateau between the two relaxation steps is barely visible in the passive case, but as activity increases the plateau disappears altogether, although the broader second relaxation can still be distinguished. At the two highest activities only a single exponential relaxation remains. The MSD mirrors the same phenomenology (Fig. 4c): the passive case displays a subdiffusive plateau, which level increases with activity until total disappearance at the two highest activities. The increase in plateau height from the passive case to $T_{\text{eff}}/T_0 = 1.4$ and 1.7 indicates wider cages.

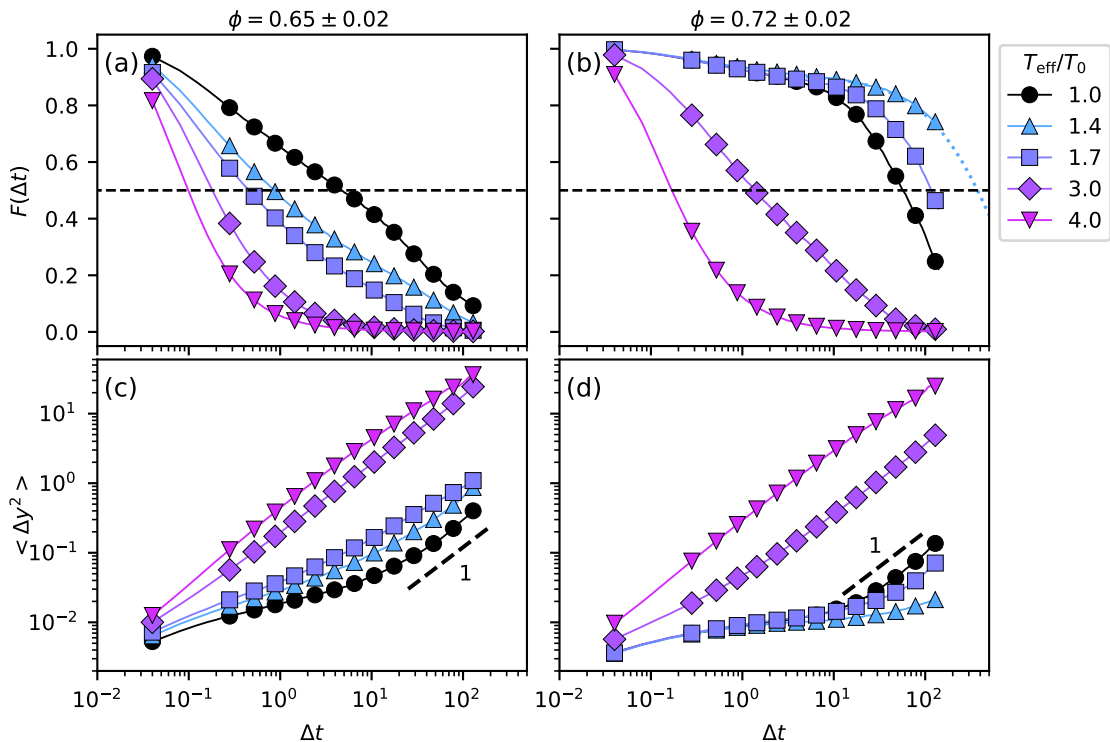


FIG. 4. Characterization of the system dynamic at two fixed densities, in the ergodic (left panel) and nonergodic (right panel) phase, and various activity levels. (a,b) Overlap function $F(\Delta t)$. Crossing of the horizontal dashed line at $F(\Delta t) = 0.5$ defines the relaxation time τ . The dotted line in (b) at $T_{\text{eff}}/T_0 = 1.4$ is the extrapolation of a stretched exponential fit of $F(\Delta t)$ to obtain τ . (c,d) MSD along y direction. The dashed line has slope one. It guides where the MSD exhibits diffusive motion.

Beyond glass transition, at $\phi = 0.72 \pm 0.02$, the dynamics of the system shows stark differences. The level of the plateau in the MSD (Fig. 4d) does not depend on activity, hinting at a constant cage size. However the exit of the plateau does depend on activity in a nonmonotonic way. $T_{\text{eff}}/T_0 = 1.4$ exits the plateau later than the passive case. The next activity exists earlier than 1.4 but still later than the passive case. The two last activities show no plateau. We thus recover the ‘back and forth’ behavior, even at constant density. The overlap function (Fig. 4b) displays a similar behavior, with superimposed plateaus but exit times that evolve nonmonotonically with activity.

In the glass, the plateaus have the same level at low activities. It means that weak self-propulsion is not enough to enlarge the accessible area. It reveals that each particle faces steep energy barriers. Particles are already as close as they can be. Since their interaction potential is steep at short distances, the extra energy afforded by $T_{\text{eff}}/T_0 < 2$ cannot push the particles significantly closer. By contrast in the supercooled regime the particles are relatively further apart, feeling a softer confinement. Therefore, even weak self-propulsion can push against these barriers and enlarge the accessible area, which shows on the increasing plateau level of MSD. To

sum up, low levels of self-propulsion enlarge the cage in supercooled regime but not in glass regime. The exit from the cage is actually delayed longer at low activities, a point that cannot be explained solely from spatially averaged dynamics.

RELAXATION MECHANISMS

To understand the origin of the nonmonotonic behavior in the nonergodic glass phase, we explore the relaxation mechanism in microscopic detail. For this, we need a rather wide slice where the volume fraction could be considered uniform and above the glass transition density of the passive case. We thus focus on a slice of width $\approx 60\sigma_0$ where the volume fraction is $\phi = 0.80 \pm 0.03$.

Since the interesting physics seems to occur at the exit of the plateau, we focus on the time scale $\Delta t = 32$ that corresponds to $F(\Delta t)$ exiting from the plateau in the passive case (not shown). We label as fast the particles that move further than the median displacement at the same T_{eff} and Δt . The other half is labeled slow. Fig. 5a shows the map of the fast and slow particles in one snapshot for $T_{\text{eff}}/T_0 = 1.7$. From this map, we can see how the fast and slow domains distribute in space. Unfortun-

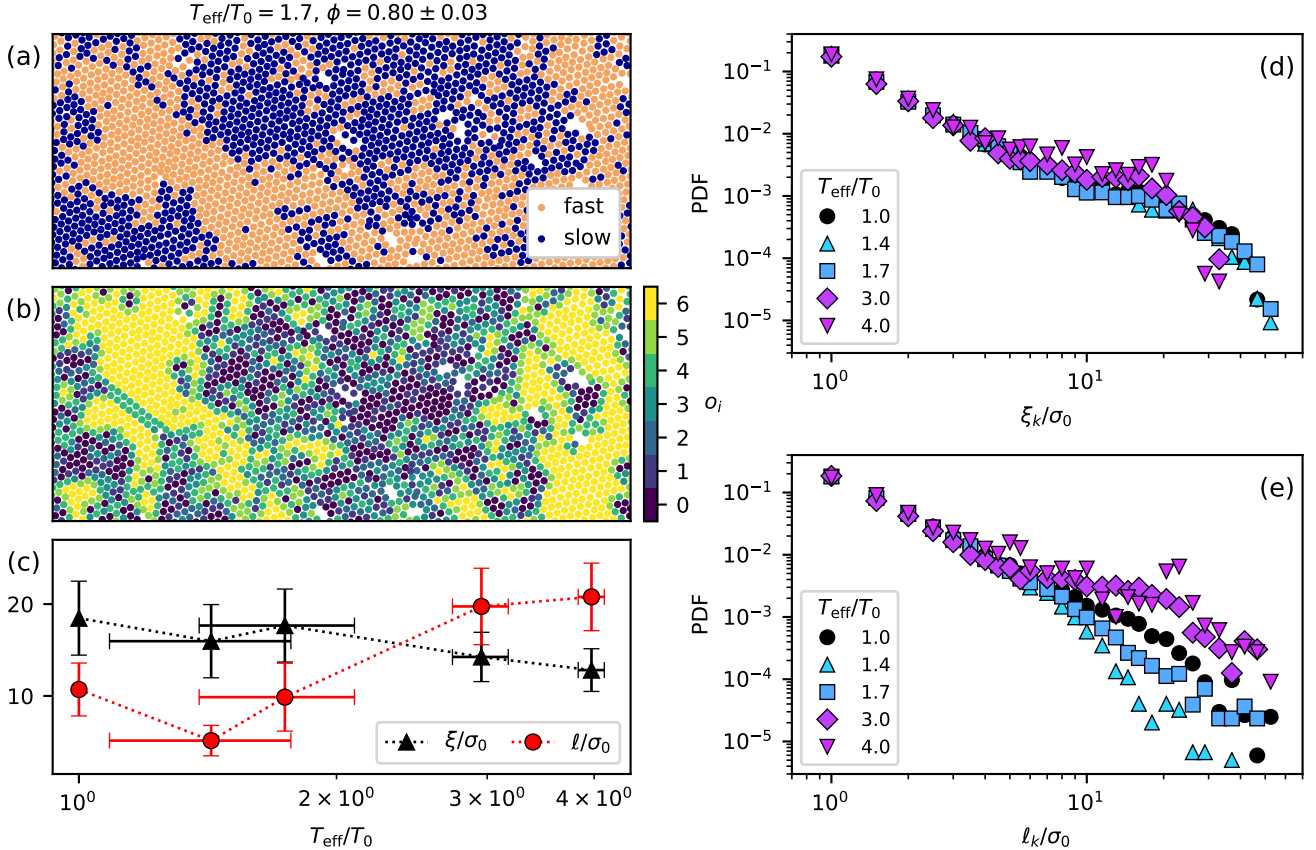


FIG. 5. (a) The fast and slow domain at $T_{\text{eff}}/T_0 = 1.7$ in the nonergodic phase (detail). Particles are split half and half between slow and fast by ranking their MSD at $\Delta t = 32$. (b) Directional correlation map at the same position and condition as (a) that shows how many neighbors of a particle i have the same displacement orientation as i . The white areas in (a) and (b) come from aggregated particles that are not tracked. (c) Average length of slow domains ξ and directional correlation domains ℓ at various T_{eff}/T_0 . (d,e) Probability distribution function (PDF) of ξ_k and ℓ_k , respectively, for each domain k at various T_{eff}/T_0 .

nately in this setup our observation window is limited by the density profile. Therefore we cannot compute long-range spatial correlation and thus we cannot extract the 4-point dynamic susceptibility or correlation length. Instead, we define a dynamic length scale as the average size of slow domains.

We define the graph of particle bonds such that each particle is bonded to its six nearest neighbors. We then take the subgraph of slow particles and split it in connected components [35]. This defines slow domains. For each slow domain k , we measure its radius of gyration in the direction perpendicular to $g \sin \theta$:

$$\xi_k = \frac{1}{N_k} \sqrt{\sum_{i \in k} y_i^2 - \left(\sum_{i \in k} y_i \right)^2}, \quad (6)$$

where N_k is the number of particles in cluster k . The probability distribution function (PDF) of ξ_k of all clusters at all time for various activities are displayed in Fig. 5d. The distributions for $T_{\text{eff}} < 2T_0$ are practically the same. The distributions of the two highest activities

are identical to the others at small size ($\xi_k < 5$) but show an excess probability at intermediate sizes ($5 < \xi_k < 20$), and less large clusters ($\xi_k > 20$). The size of slow domains thus seems sensitive to what occurs at high activity but not so much in the low activity limit.

This is confirmed by the characteristic size of slow domains, that we define by a weighted average of ξ_k on all clusters at all time:

$$\xi = \frac{\sum_{t_0} \sum_k N_k \xi_k}{\sum_{t_0} \sum_k N_k}. \quad (7)$$

In Fig. 5c we show the evolution of ξ function of T_{eff}/T_0 (black triangles). We observe a weak decreasing trend, with little difference between the passive and the low activity cases.

A large correlation length is usually associated with slower relaxation. In particular large 4-point correlations are associated with long relaxations in glassy system [17], including active supercooled liquids [24]. If we accept that our ξ qualitatively captures the dynamic correla-

tion length, a decreasing ξ between the first non-zero activity and the highest activity is consistent with the observed ‘forth’ behavior where the relaxation time decreases. However, we observe no sign of the ‘back’ behavior. The order of magnitude increase of relaxation time observed between passive and first non-zero activity does not translate into an increase of ξ .

Since the classic tools to characterize dynamical heterogeneities in isotropic system fail us, we define an other length scale as the average size of oriented domains, better adapted to describe dynamic heterogeneities emerging from directed particle motion. For each particle i , we count the number of its neighbors j that have moved to the same direction after Δt :

$$o_i = \sum_j \Theta \left(\frac{\vec{u}_i \cdot \vec{u}_j}{|\vec{u}_i| |\vec{u}_j|} - 0.5 \right), \quad (8)$$

where \vec{u}_i is the displacement. Fig. 5b shows the map of o_i for the same snapshot as in Fig. 5a. We observe that the fast domains in Fig. 5a roughly correspond to highly oriented domains in Fig. 5b. This hints toward relaxation processes where neighboring particles move together in the same direction, at least at $T_{\text{eff}}/T_0 = 1.7$. Such collective motions are characteristic of active matter.

We can define oriented domains as the connected components of the subgraph such that $o_i \geq 4$. For each oriented domain k we measure ℓ_k , its radius of gyration in the direction perpendicular to $g \sin \theta$ in the same way as (Eq. 6). We then define a characteristic size of oriented domains ℓ in the same way as (Eq. 7). As shown on Fig. 5c, ℓ displays a nonmonotonic evolution with activity consistent with the ‘back and forth’ behavior: a drop of a factor 2 from the passive case to the lowest activity, and then a progressive increase at higher activities. This trend is confirmed by the PDF of ℓ_k in Fig. 5d. For ($\ell_k < 5$), the distributions at all activities collapse. Compared to the distribution in the passive case, low activities are deprived of large oriented domains, whereas high activities have an excess probability of large oriented domains. Above $\ell_k \approx 10$ the distributions follow the ‘back and forth’ behavior.

However, the length ℓ evolves in reverse to what one would expect for a (dynamic) correlation length: large ℓ corresponds to fast relaxation. Indeed, ℓ measures the size of domains with correlated orientation of displacement, associated with collective rearrangements, whereas 4-point correlation measures the size of cooperatively rearranging regions. A large domain moving collectively in the same direction enhances relaxation, whereas a large cooperative region size implies a larger energy barrier and thus longer relaxation. This hints to the existence of relaxation mechanisms specific to self-propelled particles that involve collective directed motion instead of cooperative rearrangements.

The ‘forth’ behavior can be explained by the rise of collective motion. However the delayed exit from the

plateau, characteristic of the ‘back’ behavior occurs when collective motion is still negligible. Therefore, all our experimental results point to a drop in efficiency of cooperative rearrangements between the passive case and our lowest activities. In the following we explain analytically how a glass of weakly active Brownian particles can relax slower than a glass of passive Brownian particles, and why the transition between the two behaviors is so sudden.

ANALYTICAL MODEL

For cooperative rearrangements to occur, an energy barrier needs to be crossed. Here, we suppose that in the limit where T_{eff} is close to T_0 the extra energy provided by self-propulsion is not altering significantly the height of the energy barrier. However, the attempt frequency might be altered by the process of space exploration. Below, we replace the many particle problem by the simpler problem of a single particle that explores a cage of size $0.3\sigma_0$.

A Brownian particle of mass m and mobility $\mu = 6\pi\eta R_H$ explores its cage by diffusion in a time $\tau_{\text{cage}}^B = (0.3\sigma_0/R_H)^2 \tau_T \approx 0.1\tau_R$. A particle submitted only to a self-propulsion force F_P following (Eq. 1) and with a 3D reorientation time τ_R , explores space by a persistent random walk of persistence time $\tau_R/2$ [5, 26]. Here the persistent length is longer than the size of the cage, thus the elementary time of cage exploration is $\tau_{\text{cage}}^P = \tau_R/2$. It implies that $\tau_{\text{cage}}^P/\tau_{\text{cage}}^B \approx 5$. A nonBrownian self-propelled particles explores its cage five times slower than a Brownian particle.

Experimentally, our particles are submitted to both translational Brownian motion and propulsion forces. For times shorter than the persistence time, a particle thus undergoes random motion biased in the propulsion direction. This situation is analogous to the sedimentation-diffusion problem [31], replacing the weight by the propulsion force. Along the propulsion direction, the particle probability density follows an exponential law of characteristic length $\lambda_P \equiv k_B T_0 / F_P$, analogous to a sedimentation length. Combining (Eq. 1) and (Eq. 3) we get the relevant Peclet number for cage exploration

$$\text{Pe} \equiv \frac{0.3\sigma_0}{\lambda_P} = \frac{3}{\sqrt{2}} \frac{0.3\sigma_0}{R_H} \left(\frac{T_{\text{eff}}}{T_0} - 1 \right)^{1/2}. \quad (9)$$

The propulsion force dominates the cage exploration for $\text{Pe} > 1$, that occurs above the effective temperature $T_{\text{eff}}^*/T_0 = 1 + (2/9)(R_H/0.3\sigma_0)^2 \approx 1.45$, that corresponds to the lowest activity we can achieve experimentally. Therefore, even at our lowest nonzero activity, diffusion is facing an uphill battle to explore the cage in the direction against propulsion. There is thus a practical discontinuity between our passive case, where the cage is explored

by translational Brownian motion, and our first active case ruled by the physics of self-propelled particles. Between these two cases, the attempt frequency to cross energy barriers in the glass phase is reduced by a factor of 5.

DISCUSSION AND CONCLUSION

We have found experimentally that the approach to glass transition in an active system could be mapped onto the behavior of a passive supercooled liquid of soft colloids. However, we have observed the failure of this mapping beyond the glass transition, characterized by a nonmonotonic response of the relaxation time to an increase of effective temperature. We attribute the failure of this mapping to a drop in the efficiency of cooperative relaxation modes between passive and low-activity cases. This drop can be at least partly understood in terms of efficiency of space exploration between Brownian and self-propelled particles.

The magnitude of the observed slowdown is larger than the factor of 5 found by our analytical model taking into account space exploration of a single particle. We conjecture that the many-body nature of cooperative motion has to be taken into account to quantitatively predict the magnitude of the slowdown. A reduction in attempt frequency at the single-particle scale may translate nonlinearly into a larger relaxation time at the level of the cooperative region. Unfortunately recent extensions of glass theories to active matter rely explicitly on effective single-particle models [25]. Furthermore, we have to take into account that the number of degrees of freedom per particle jumps from 2 in the Brownian case, to 3 in the self-propelled case where orientation become important. In other words, directional motion adds N degrees of orientational freedom that increase even more the complexity of the landscape and slows down relaxation. Our analytical argument on propulsion-induced confinement shows that the switch from isotropic to oriented system is effective at very low activities.

The authors thank Ludovic Berthier, Grzegorz Szamel, Chandan Dasgupta and Takeshi Kawasaki for fruitful discussions. N.K. is supported by PhD scholarship from the doctoral school of Physics and Astrophysics, University of Lyon. N.K. and M.L. acknowledge funding from CNRS through PICS No 7464. M.L. acknowledges support from ANR grant GelBreak ANR-17-CE08-0026. C.C.B. and C.Y. acknowledge support from ANR-16-CE30-0028 and from Université de Lyon, within the program Investissements d’Avenir (ANR-11-IDEX-0007) operated by the French National Research Agency (ANR).

-
- * Now in: Fachbereich Physik, Universität Konstanz, Universitätsstrasse 10, 78464 Konstanz, Germany
 † cecile.cottin-bizonne@univ-lyon1.fr
- [1] M. Ballerini, N. Cabibbo, R. Candelier, A. Cavagna, E. Cisbani, I. Giardina, V. Lecomte, A. Orlandi, G. Parisi, A. Procaccini, M. Viale, and V. Zdravkovic, *Proc. Natl. Acad. Sci.* **105**, 1232 (2008).
 - [2] M. C. Marchetti, J. F. Joanny, S. Ramaswamy, T. B. Liverpool, J. Prost, M. Rao, and R. A. Simha, *Reviews of Modern Physics* **85**, 1143 (2013).
 - [3] C. Bechinger, R. Di Leonardo, H. Löwen, C. Reichhardt, G. Volpe, and G. Volpe, *Rev. Mod. Phys.* **88**, 045006 (2016).
 - [4] É. Fodor and M. C. Marchetti, *Physica A: Statistical Mechanics and its Applications* **504**, 106 (2018).
 - [5] J. Palacci, C. Cottin-Bizonne, C. Ybert, and L. Bocquet, *Phys. Rev. Lett.* **105**, 088304 (2010).
 - [6] Y. Fily and M. C. Marchetti, *Phys. Rev. Lett.* **108**, 235702 (2012).
 - [7] A. Wysocki, R. G. Winkler, and G. Gompper, *EPL (Europhysics Letters)* **105**, 48004 (2014).
 - [8] P. Digregorio, D. Levis, A. Suma, L. F. Cugliandolo, G. Gonnella, and I. Pagonabarraga, *Phys. Rev. Lett.* **121**, 098003 (2018).
 - [9] G. Briand, M. Schindler, and O. Dauchot, *Phys. Rev. Lett.* **120**, 208001 (2018).
 - [10] J. Deseigne, O. Dauchot, and H. Chaté, *Phys. Rev. Lett.* **105**, 098001 (2010).
 - [11] I. Theurkauff, C. Cottin-Bizonne, J. Palacci, C. Ybert, and L. Bocquet, *Phys. Rev. Lett.* **108**, 268303 (2012).
 - [12] F. Ginot, I. Theurkauff, F. Detcheverry, C. Ybert, and C. Cottin-Bizonne, *Nature Communications* (2018), 10.1038/s41467-017-02625-7.
 - [13] A. Bricard, J.-B. Caussin, N. Desreumaux, O. Dauchot, and D. Bartolo, *Nature* **503**, 95 (2013).
 - [14] D. Nishiguchi and M. Sano, *Phys. Rev. E* **92**, 052309 (2015).
 - [15] L. Berthier, E. Flenner, and G. Szamel, *New J. Phys.* **19**, 125006 (2017).
 - [16] N. Klongvessa, F. Ginot, C. Ybert, C. Cottin-Bizonne, and M. Leocmach, arXiv:1902.01746 [cond-mat] (2019), arXiv:1902.01746 [cond-mat].
 - [17] A. Cavagna, *Physics Reports* **476**, 51 (2009).
 - [18] P. Charbonneau, J. Kurchan, G. Parisi, P. Urbani, and F. Zamponi, *Annual Review of Condensed Matter Physics* **8**, 265 (2017).
 - [19] R. Ni, M. A. C. Stuart, and M. Dijkstra, *Nature communications* **4**, 2704 (2013).
 - [20] F. Ginot, I. Theurkauff, D. Levis, C. Ybert, L. Bocquet, L. Berthier, and C. Cottin-Bizonne, *Phys. Rev. X* **5**, 011004 (2015).
 - [21] B. ten Hagen, S. van Teeffelen, and H. Löwen, *Journal of Physics: Condensed Matter* **23**, 194119 (2011), arXiv:1005.1343.
 - [22] L. Berthier, *Phys. Rev. Lett.* **112**, 220602 (2014).
 - [23] G. Szamel, E. Flenner, and L. Berthier, *Phys. Rev. E* **91**, 062304 (2015).
 - [24] E. Flenner, G. Szamel, and L. Berthier, *Soft Matter* **12**, 7136 (2016).
 - [25] S. K. Nandi, R. Mandal, P. J. Bhuyan, C. Dasgupta, M. Rao, and N. S. Gov, *Proceedings of the National*

- Academy of Sciences (2018).
- [26] J. R. Howse, R. A. L. Jones, A. J. Ryan, T. Gough, R. Vafabakhsh, and R. Golestanian, *Phys. Rev. Lett.* **99**, 048102 (2007).
- [27] D. Allan, T. Caswell, N. Keim, and C. van der Wel, “trackpy: Trackpy v0.3.2,” (2016).
- [28] W. F. Paxton, K. C. Kistler, C. C. Olmeda, A. Sen, S. K. St. Angelo, Y. Cao, T. E. Mallouk, P. E. Lammert, and V. H. Crespi, *Journal of the American Chemical Society* **126**, 13424 (2004).
- [29] A. Brown and W. Poon, *Soft Matter* **10**, 4016 (2014).
- [30] E. R. Weeks, J. C. Crocker, A. C. Levitt, A. Schofield, and D. A. Weitz, *Science* **287**, 627 (2000).
- [31] J. Perrin, *Ann. Chim. Phys.* **18**, 5 (1909).
- [32] J. Tailleur and M. E. Cates, *EPL* **86**, 60002 (2009).
- [33] E. Flenner, M. Zhang, and G. Szamel, *Phys. Rev. E* **83**, 051501 (2011).
- [34] A.-M. Philippe, D. Truzzolillo, J. Galvan-Myoshi, P. Dieudonné-George, V. Trappe, L. Berthier, and L. Cipelletti, *Phys. Rev. E* **97**, 040601(R) (2018).
- [35] A. A. Hagberg, D. A. Schult, and P. J. Swart, in *Proceedings of the 7th Python in Science Conference*, edited by G. Varoquaux, T. Vaught, and J. Millman (Pasadena, CA USA, 2008) pp. 11 – 15.